Customized MFM probes based on magnetic nanorods

Miriam Jaafar*[a,b], Javier Pablo-Navarro[c], Eider Berganza[b,d], Pablo Ares[a], César Magén[c,e,f], Aurélien Masseboeuf[g], Christophe Gatel[g], Etienne Snoeck[g], Julio Gómez-Herrero[a], José María de Teresa[c,e,f], Agustina Asenjo[b]

Focused Electron Beam Induced Deposition (FEBID) for magnetic tip fabrication is presented in this work as an alternative to conventional sputtering-based Magnetic Force Microscopy (MFM) tips. FEBID enables the growth of a high-aspect-ratio magnetic nanorod with customized geometry and composition to overcome key technical limitations of MFM probes currently in the market. The biggest asset of these tips, in comparison to the CoCr coated pyramidal probes, lies on the capability of creating sharp ends, nearly 10 nm in diameter, which provides remarkable (topographic and magnetic) lateral resolution in samples with magnetic features close to the resolution limits of the MFM technique itself. The shape of the nanorods produces a very confined magnetic stray field, whose interaction with the sample is extremely localized and perpendicular to the surface, with negligible in-plane components. This effect can lead to a better analytical and numerical modelling of the MFM probes and to an increase of sensitivity without perturbing the magnetic configuration of soft samples. Besides, the high-aspect ratio achievable in FEBID nanorod tips makes them magnetically harder than the commercial ones, reaching coercive fields higher than 900 Oe. According to the results shown, tips based on magnetic nanorods grown by FEBID can be eventually used for quantitative analysis in MFM measurements. Moreover, the customized growth of Co or Fe based tips onto levers with different mechanical properties allows MFM studies that demand different measuring conditions. To showcase the versatility of this type of probes, as a last step, MFM is performed in liquid environment, which still remains a challenge for the MFM community largely due to the lack of appropriate probes in the market. This opens up new possibilities in the investigation of magnetic biological samples.

Introduction

Magnetic Force Microscopy (MFM) is a variant of the Atomic Force Microscopy (AFM) used to study magnetic structures at the nanoscale [1-3]. A magnetized tip at the end of a microcantilever scans a sample and detects the tip-sample magnetic interactions. MFM tips generally consist of standard AFM probes with a sputtered magnetic coating. Despite the many improvements achieved by the MFM community throughout the years, the intrinsic drawback of this approach is the increase of the final tip radius and a weak control of the magnetic coating influence over the sample magnetic state. Since the invention of Scanning Probe Microscopy (SPM) techniques, research groups [4-7], as well as commercial companies have offered different solutions to improve resolution and sensitivity and, in the particular case of the MFM, the magnetic stray field created by the tip, which determines the strength of the tip-sample magnetic interaction. The general trend is to deposit a large amount of magnetic material at the tip apex to improve the signal-to-noise ratio (SNR). However, the drawback of this approach is that the wider the magnetic probe the lower the lateral resolution and the higher its influence over the sample magnetic state. Another critical parameter to get high SNR is the cantilever geometry whose mechanical properties control the magnetic sensitivity.

In the present work, we explore the optimization of MFM probes for different applications by means of the fabrication of Focused Electron Beam Induced Deposition (FEBID) magnetic nanorods on top of a non-magnetic AFM tip.

FEBID growth of nanorods on tips has already been used for different applications such as photon scanning tunnelling microscopy (PSTM) [8], magnetic force sensing [9], ferromagnetic resonance force microscopy (FMRM) [10] and MFM applications [11-13]. In the latter case, previous work focused on the lateral resolution and the importance of the tilt angle of the magnetic tip with respect to the scanned sample were performed [14], but no systematic studies on the impact of the type of FEBID tip on the stray field and the sensitivity in MFM experiments were carried out.

We demonstrate that tuning the geometry and the composition of the magnetic nanorod tip allows controlling the sensitivity, the lateral resolution and the stray field created by the probe. The FEBID technique is therefore an alternative nanofabrication method of MFM probes compared to the standard ones based on sputtering deposition (used by the companies) and to other sophisticated non-commercial probe fabrication methods [15-16]. The main advantage of magnetic FEBID tips [17] is the possibility to adapt the magnetic probe to the experimental needs at a competitive cost.

In addition to the choice of the FEBID magnetic nanorod material, length and diameter, the MFM probe system can be tuned by choosing the cantilever on which the nanorod is grown to achieve the most favourable mechanical properties according to the environment and operating modes of the targeted experiment. In the present work, we demonstrate that the appropriate combination of magnetic nanorod-tip and cantilever leads to high-quality images in different environmental conditions, from vacuum to liquid media. In fact,

our results highlight that the strategy of using MFM nanorod tips gives rise to outstanding performance in liquid environment, for which no commercial alternatives are available. These findings open up new avenues for investigating biological samples in a physiological medium, a key aspect for the development of new applications in nanobiology and nanomedicine.

Nanorod-tip fabrication

Magnetic nanorods of different materials can be fabricated through FEBID [18,19] with remarkable control over the nanorod position on the cantilever, geometrical parameters [20] and material features in terms of composition and crystallinity [21].

Brand	*Tip side coating*	*Resonance frequency* (kHz)	*Force Constant* (N/m)	*Length* (µm)	*Width* (µm)
Nanoworld-Arrow EFM	PtIr	75	2.8	240	35
Budget Sensors ElectriMulti75-G	CrPt	75	3	225	28
Bruker Rocky Mountain	Solid Pt	10	8	400	100
Olympus BioLever mini	Si	110 (in air) 25 (in water)	0.09	38	16

Table 1: Main characteristics of the commercial cantilevers used for the growth of the nanorods.

Three-dimensional (3D) Co- and Fe-based FEBID nanorods have been grown onto SPM probes, as shown in Figure 1.
Four different kinds of cantilevers were used: Nanoworld-Arrow EFM, Budget Sensors, Bruker Rocky Mountain and Olympus BioLever mini (see Table 1). No charge effect due to the electron-beam was found during the FEBID growth, except for the Olympus BioLever mini cantilever. In order to avoid it, a C adhesive tape was used underneath and over few areas of the cantilever to achieve more efficient charge dissipation.

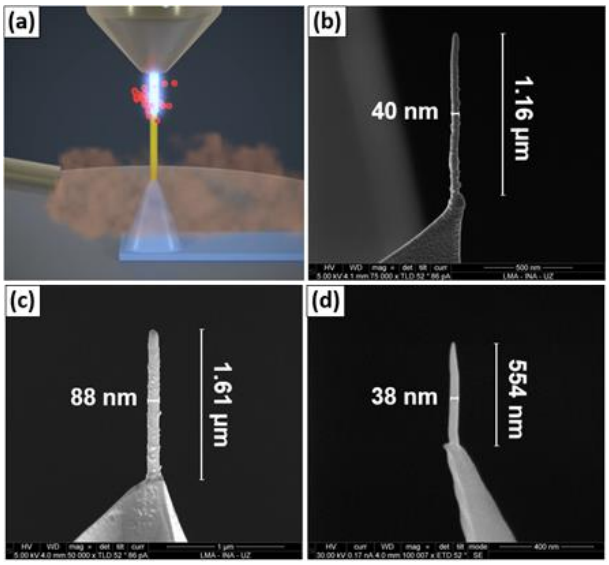

Figure 1. (a) Diagram of the FEBID process. SEM images of magnetic nanorods grown on various commercial cantilevers: (b) Nanoworld-Arrow EFM, (c) Budget Sensors ElectriMulti75 and (d) Olympus Biolever mini AFM probes, with their corresponding (b, c) Co- and (d) Fe-based nanorods.

Experimental Results

We firstly analysed Fe- and Co-based magnetic FEBID tips grown on non-magnetic cantilevers (*Nanoworld Arrow EFM*) of similar properties, i.e., resonance frequency and spring constant of 75 kHz and 3 N/m, respectively. The performance of the nanorods has been compared to that of standard tips using a high-density hard disk as a reference sample. Although some works used magnetic nanoparticles [22] to model the probe–sample interaction, this reference sample is the most frequently used in the literature for the calibration of MFM probes [5]. Figure 2 shows the topographic and magnetic images obtained with these probes. It is noteworthy that in both cases, Fe- and Co-based FEBID tips exhibit similar behaviour to that of a commercial tip with a 50-nm-thick CoCr coating (*Budget Sensors MagneticMulti75-G*) but with less amount of magnetic material and therefore with a weaker influence on the magnetic state of the sample. The MFM signal is presented in units of hertz (Hz) corresponding to the frequency shift due to the magnetostatic interaction between the tip and the sample. The positive MFM contrast represents a repulsive interaction, while the negative signal is due to an attractive interaction.

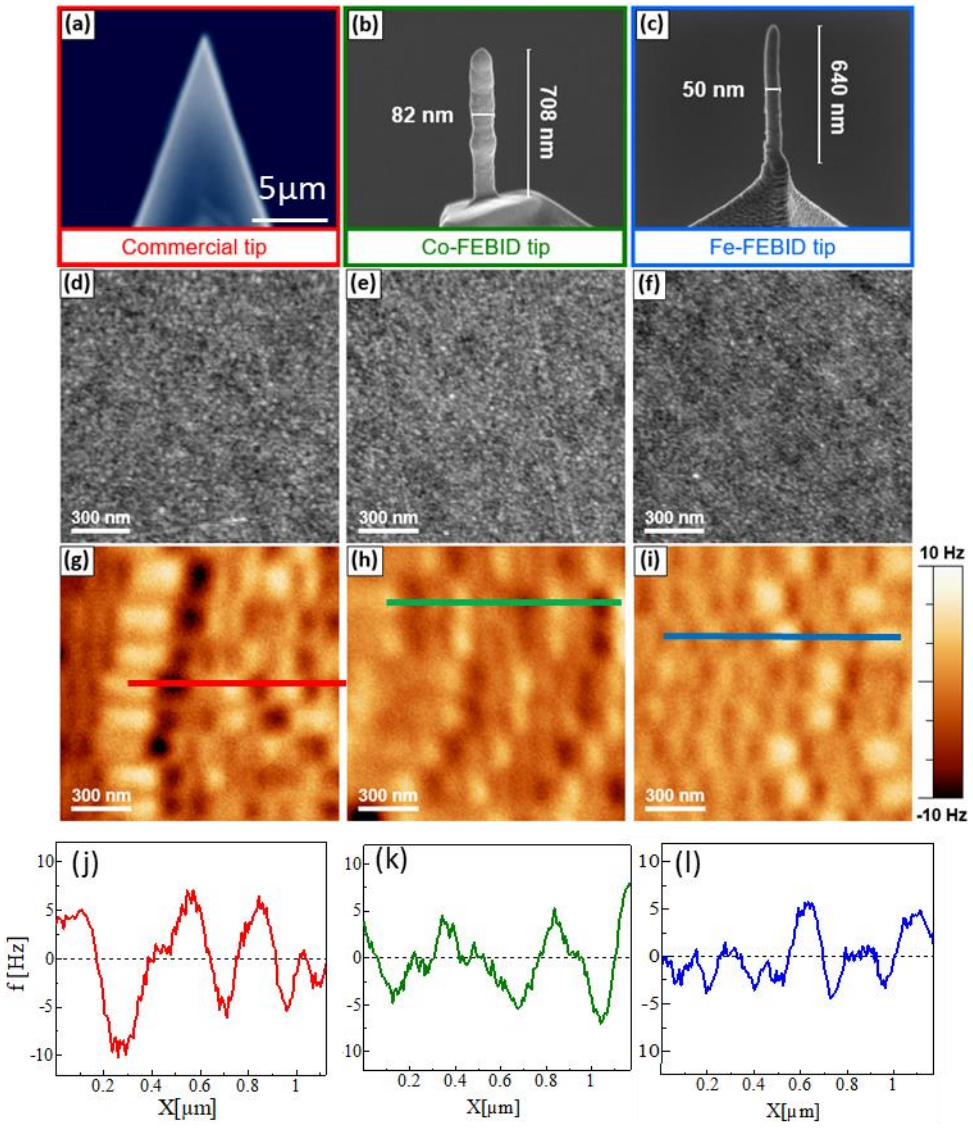

Figure 2. Images of (a) Commercial *Budget Sensors MFM* tip with 50 nm of CoCr coating, (b) Co-based FEBID tip and (c) Fe-based FEBID tip grown on *Nanoworld Arrow EFM* cantilevers. (d,e,f) Topographic images of a hard disk reference sample obtained by the selected MFM probes and (g,h,i) their corresponding magnetic images and profiles (j,k,l) respectively. Z lift was 30 nm in all cases.

MFM tips with high coercive field are required to avoid artefacts coming from the switching of the magnetization of the probes when scanning the magnetic sample to perform stable MFM measurements. Local hysteresis loops of the FEBID probes have been measured using a non-conventional advanced MFM-based method previously reported [4,23] (see Supporting Information SI1 for more details). The coercive field measured by applying the magnetic field parallel to the nanorod long axis is about 550-600 Oe for the case of Co-based nanorods, similar to the one shown in Figure 2b, and higher than 900 Oe for Fe-based nanorod tips like the one in Figure 2c. In comparison, the commercial tips display much lower coercivity values, typically around 200 Oe (*MFM Team Nanotec*) and 350 Oe (*Budget Sensors MagneticMulti75-G*). We believe that the high aspect ratio achievable in FEBID tips makes them magnetically harder than the commercial ones. This is especially useful to achieve reliable results when applying *in-situ* magnetic fields or when measuring samples with a very high stray field [24], as it will allow measurements up to higher fields without artefacts due to modifications of the tip magnetic state.

In addition, different MFM experiments were carried out to explore the customization of the tip stray field by accurately controlling the nanorod-tip dimensions. Standard MFM imaging only provides qualitative information about the magnetic configuration of the sample. In fact, the MFM signal is proportional to the second-order derivative of the interaction between the magnetic stray field of the tip and the sample. To gain quantitative information from the MFM signal, the tip stray field can be calibrated [25] by measuring the frequency shift experimented by the oscillating cantilever when the tip approaches the surface of a reference sample. The frequency shift is proportional to the magnetic moment of the tip [3]. A comparison between Fe-based FEBID tips with different apex radius and a standard commercial tip (Budget Sensors MagneticMulti75-G) has been performed using a FePd multilayer [26] displaying perpendicular maze domains as a reference sample (see Figure 3). To optimize the signal of the probes, 1-µm-long Fe-based nanorods with different tip apexes were prepared. As shown in Figure 3a, the image obtained with a commercial tip presents a maximum MFM contrast of around 55 Hz (this value can be used to estimate its stray field); the jumps or spikes in the image (Figure 3b) are due to the tip influence on the sample configuration [27]. The nanorod tip with 50 nm in diameter and blunt shape gives a frequency shift of ~40 Hz, whereas a narrower nanorod (32 nm in diameter) with sharper apex (final tip diameter about 7 nm) gives ~15 Hz of contrast. It is noticeable that there are no irreversible changes in the magnetic configuration of the sample when the sharper apex tip is used (Figure 3d). Moreover, the lateral resolution is also improved (see Supplementary Information SI2 where the finest nanorod has been used to image a soft magnetic nanodot whose interaction with the probe is very critical). In brief, the sharp geometry is useful to perform very high resolution MFM imaging as well as to obtain a low tip-sample interaction, minimizing the influence of the tip on the magnetic state of the sample [28].

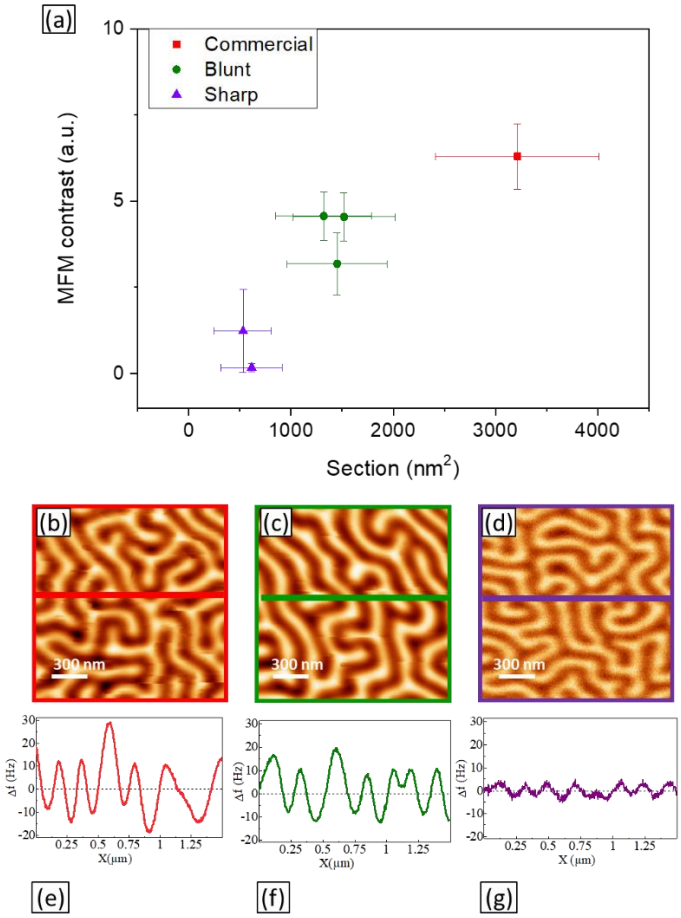

Figure 3. (a) Measurement of the MFM contrast, related to the tip stray field, for the three tips investigated, represented as a function of the magnetic tip section. The corresponding MFM images and profiles, performed with (b)-(e) a standard commercial MFM probe (red), (c)-(f) a tip fabricated with an Fe-based FEBID nanowire with a blunt tip end of 50 nm (green) and (d)-(g) a narrower nanorod (32 nm in diameter and

a sharp tip end of 7 nm (purple), are shown. The sample is a FePd multilayer with perpendicular maze domains and the magnetic images were acquired at a 10nm Z lift distance.

One Fe-based nanorod with sharp tip end was selected to perform on it comprehensive local chemical and magnetic analyses. As reported in Figure 4a, using Scanning Transmission Electron Microscopy (STEM) imaging and Electron Energy Loss Spectroscopy (EELS) we can plot the STEM-EELS compositional profile along the length of the nanorod as a function of the distance to the tip apex reveals that the Fe content is decreasing close to the tip apex. The Fe content decreases from 70% in the central region of the nanorod to about 20% at 3.5 nm from the tip apex where a 3 nm thick oxidation layer is observed. A STEM-EELS chemical map is depicted in Figure 4a (top inset) for an easier comparison with the results extracted from TEM imaging and Electron Holography (EH) experiments.

As illustrated in Figure 4, the local magnetic characterization by EH allows mapping and quantifying not only the magnetic induction inside of the specimen (~0.7 T in the central region) but also the magnetic stray field as a function of the distance to the apex. The pure magnetic component of the phase shift has been recovered using the time reversal method [29]. This is particularly useful for the development of quantitative MFM measurements. The magnetic flux lines (Figure 4b) indicate that the magnetization is homogeneous and maximum within the central part of the nanorod and runs parallel to it (as expected due to the shape anisotropy) and decreases close to the tip, giving rise to smaller stray fields. Therefore, the tip shape has a significant impact on the magnetic stray fields generated in the surroundings of the nanorod-tip as deduced from the comparative study of 5 different nanorods presented in Figure S3 of the Supplementary Information SI3. The EH measurements show that the stray field at the apex is determined by the shape of its very end, while the stray field at the MFM typical working distance is related to the section of the nanorod. To overcome the signal integration that is made in TEM we used the cylindrical symmetry of the wire and the Abel transform (see ref. [30] for details) to obtain a quantitative value of the field (Figure 4c) at the apex only. As one might see, the values that are obtained with conventional measurement on the phase (dashed lines) are overestimating such magnetic stray field (as well as underestimating the magnetization in the nanorod). The magnetic field at the apex of the tip is as high as 800 Oe and drops to 350 Oe after 50 nm (typical distance for the MFM measurement).

It has to be emphasized that thanks to the cylindrical geometry of the nanorods, the van der Waals (vdW) interaction between the tip and the sample surface is lower than for wider probes (see Supporting Information SI4). The low vdW probe-sample interaction presents two main advantages. It first allows measuring the magnetic properties of the sample much closer to its surface and therefore permits the measurement of lower magnetic induction, which cannot be detected with conventional magnetic probes scanning at a larger distance from the surface. Second, the mapping of the stray field emanating from the sample is better localized since the cylindrical geometry and the high aspect ratio of the nanorods maximize the Out-Of-Plane (OOP) vs. In-Plane (IP) stray field ratio (as shown in Supporting Information SI5). Such nanorod specificities are particularly essential to avoid the alteration of domain structures in soft in plane magnetic materials and for future quantitative studies.

Finally, it is worth stressing the versatility of this nanoprobe preparation procedure. In the experiments shown above we focused on the properties of the nanorods and their weak influence on the tip-sample interaction. However, the SNR measurement depends both on the environment and the cantilever properties, thus we explored the possibility of growing nanorods on different kinds of cantilevers. The lever force constant constitutes another degree of freedom when choosing a probe for an AFM/MFM measurement. Mechanically soft samples require low force constant microcantilevers to avoid structural damage, while harder cantilevers provide better stability during the measurement, but at the expense of a stronger interaction (a detailed description of the enhancement of the SNR can be found in Supporting Information SI6). Additionally, several works are aimed to pave the way to the applicability of MFM for the study of magnetic nanostructures in liquid environments [31,32,33]. In the most recent studies, reasonable lateral resolution as well as enough SNR were achieved by working in DAM-AFM (Drive-Amplitude Modulation mode [34]). In terms of the acquisition of magnetic interactions, DAM-AFM is the same as Frequency Modulation FM-AFM, but since in DAM-AFM there are no frequency shift contributions to the topography, it has the advantage of no magnetic cross-talk in the first pass topography acquisition.

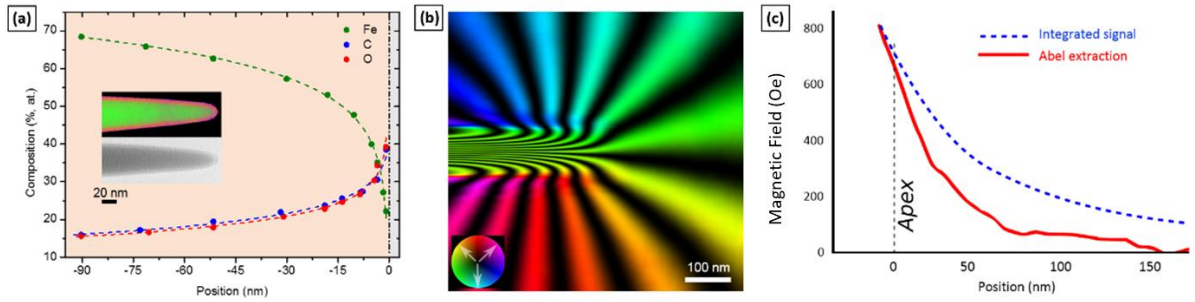

Figure 4. (a) STEM-EELS chemical profile of a Fe-based nanorod grown on top of an AFM probe. The vertical short dash-dot line represents the nanorod apex edge. The top inset is a chemical map showing the relative composition of Fe, C and O contents in green, blue and red, respectively. The bottom inset is the corresponding TEM image. (b) Cosine Color map: composite image displaying the magnetic field in and outside the tip using a colour scale for the direction and intensity of the integrated magnetic induction composed with the phase signal (black lines) displayed with a cosine for highlighting the magnetic flux. (c) Quantitative decay of the magnetic induction component parallel to the nanorod axis as a function of the distance from the apex determined directly from the magnetic phase image in (b) (dashed blue line), and using the Abel transform (bold red line).

However, the quality of the images was still far from those obtained in air conditions, mainly due to the low oscillation quality factor of the cantilevers in liquid environments, an intrinsic limitation of the technique. To enhance the SNR, the development of suitable MFM probes would be necessary.

Companies commercialize specific cantilevers for AFM liquid experiments, which are typically characterized by a very short and narrow lever. For example, the Biolever mini (length~38µm, width~16µm) gives rise to a low force constant of ~0.1 N/m and 110 kHz resonance frequency in air.

Coating this kind of cantilevers by conventional sputtering deposition to perform MFM experiments can be problematic, as, even if they provided enhanced performance in air measurements [35], the mechanical stability of the coating is not so strong under liquid conditions. As reported in Figure 5, a significant enhancement of the magnetic signal is obtained in liquid with a FEBID nanorod grown onto a Biolever mini in comparison with MFM data taken with commercial probes. The FEBID nanorod yields an improvement of the SNR by a factor of ~4 for these probes, in good agreement with our previous estimation of MFM noise (see [32] for more details). It is worth noting that the quality of the MFM images acquired in liquid with the FEBID nanorod is close to those acquired in air ambient conditions. As explained in Supporting Information SI4, imaging under water allows to performing the retrace closer to the surface without topographic crosstalk, which leads to higher magnetic signal values. In both experiments MFM imaging was performed in the dynamic mode DAM-AFM. Furthermore, we performed control experiments after the measurements in water to corroborate that the magnetic signal is not impaired by the effect of oxidation. Nevertheless, in some experiments it could be necessary to protect the magnetic nanorod. In that case, it is possible to grow a core-shell structure that can protect the ferromagnetic nanorod with a Pt-C coating [18] with the aim of minimizing the degradation of the magnetic properties due to the surface oxidation. (See Supporting Information SI7).

FEBID nanorods grown on cantilevers with low force constants are therefore a promising option for measuring fragile biomagnetic samples in liquid, as they can be helpful to enhance the SNR of low interacting samples. The achievement of high-quality probes for MFM measurements in liquid is of uttermost importance to strengthen the experimental capabilities of biomagnetism. So far, studies related to the performance of magnetic nanoparticles for hyperthermia [36] are performed macroscopically. Recent developments on microfluidics allow controllably inserting nanoparticles in a single cell [37]. This would allow studying, for example, the functionality of nanoparticles *in vitro*, tracking the changes in a single cell, which should be carried out in a liquid environment.

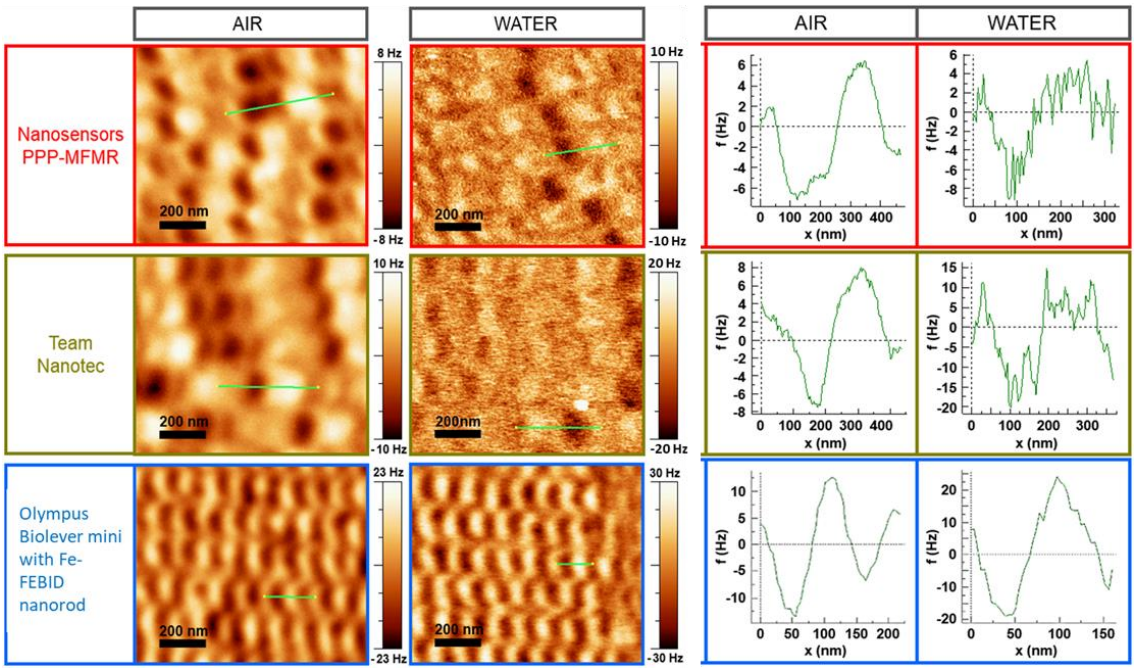

Figure 5. Comparison of the MFM images of a magnetic hard disk acquired in air and water environments with the commercial *Nanosensors PPP-MFMR* and *Team Nanotec* tips, and with the functionalized *Olympus BioLever mini* on which an Fe-based FEBID nanorod was grown. MFM signal profiles in the right panel are obtained from the green lines depicted for each tip case in the left panel. All the images were acquired in drive amplitude modulation mode, DAM-AFM. In the MFM images taken in ambient air conditions the Z lift was 20 nm whereas for the images taken in liquid the Z lift was 10 nm.

Conclusions

Summarizing, magnetic nanorods have been successfully grown onto different types of commercial AFM probe cantilevers in a reproducible way. Compared to conventional magnetic thin films sputtered onto pyramidal AFM tips, the magnetically active area is confined into the nanorod with a weaker radial stray field component. This makes these probes more reliable for quantitative MFM measurements and more suitable for the interpretation of the sample magnetic configurations. Remarkably, the nanorods are magnetically harder than average commercial MFM tips, which is a highly desirable feature for MFM measurements under in-situ applied field experiments.

The aspect ratio and sharp tip endings of the nanorods lead to improved topographical and magnetic lateral resolutions, required to measure strikingly soft or very small magnetic nanoparticles.

The versatility of this method allows the user to customize a suitable tip for a specific experiment, choosing the desired probe features, such as the nanorod material or dimension. Moreover, the nanorods can be grown with outstanding adapted mechanical stability in cantilevers of different elastic constant, opening a showcase of possibilities for measuring from mechanically hard samples to biological fragile specimens containing magnetic material. A perfect illustration of one of the most notable achievements of these new MFM sensors has been displayed with the Fe-based tips with a 7 nm sharp apex which have proven to increase by a factor of 4 the SNR of commercially MFM tips in liquid environment. This paves the way to carry out relevant experiments for biomedicine, in a suitable environment for the specimens.

Methods

Structural studies of the tips were carried out by Transmission Electron Microscopy (TEM) using an FEI Titan Cube 60-300 operated at 300 kV, and equipped with a Field Emission Gun (FEG), a Cs corrector for the objective lens and a Gatan Ultrascan 2k x 2k CCD camera. Scanning Transmission Electron Microscopy (STEM) imaging and Electron Energy Loss Spectroscopy (EELS) chemical analyses were performed in a Titan Low Base 60-300 operated at 300 kV fitted with a high-brightness FEG, a Cs corrector for the probe and a Gatan Tridiem 866 ERS spectrometer. STEM-EELS experiments were performed with a probe convergence semi-angle of 25 mrad, an energy dispersion of 0.8 eV, an energy resolution of ~1.5 eV, a pixel time of 10-20 ms and an estimated beam current of ~250 pA. The local magnetic characterization for quantitative measurements of the magnetic stray field [38] were performed by EH in a Hitachi I2TEM.

The MFM measurements were performed at ambient conditions and under liquid using a scanning force microscope from Nanotec Electronica in the amplitude modulation mode and with a phase-locked loop (PLL) enabled to track the resonance frequency [39]. Different kinds of cantilevers have been used as mentioned along the text. In most of the experiments the Z lift is 30 nm. Two reference samples have been used to analyse the in-Plane and outof-plane components of the MFM signal: a hard disk with in plane domains and an FePd sample with perpendicular anisotropy.

The 3D nanorods have been fabricated in commercial Helios Nanolab 600 and 650 Dual Beam systems using $Co_2(CO)_8$ and $Fe_2(CO)_9$ precursor gases and using electron beam voltages in the range of 3 to 30 kV. The Co-based deposits were grown with an electron beam current varying between 50 and 100 pA and a chamber growth pressure of ~9×10^{-6} mbar (base pressure of ~1.4×10^{-6} mbar). For the growth of Fe-based nanorods, the electron beam current was varied between 43 to 86 pA and the chamber growth pressure was of ~6×10^{-6} mbar.

Conflicts of interest

There are no conflicts to declare.

Author Contributions

M.J., J.M.D.T. and A.A. conceived the project. M.J. performed the MFM measurements at ambient conditions. M.J., E.B. and P.A. performed the MFM experiments in liquid environment with the help of J.G.H.. M.J. with the help of A.A. performed the analysis of the MFM data. J.P.N. fabricated the FEBID MFM tips. E.B. fabricated MFM tips by sputtering. J.P.N. and C.M. performed the TEM measurements. J.M.D.T. and C.M. supervised the growth of the MFM tips by FEBID and the TEM experiments. A.M., C.G. with the help of E.S. conducted the compositional analysis, the E.H. experiments and the analysis of the data. M.J., J.P.N, J.M.D.T and A.A. wrote the manuscript. All authors have given approval to the final version of the manuscript.

Acknowledgements

The authors acknowledge Dr. Maite Goiriena-Goikoetxea and Dr. Alfredo García-Arribas for the samples. M.J., E.B. and A.A. acknowledge the support from Spanish Ministry of Economy and Competitiveness (MINECO) under projects no. MAT2015-73775-JIN and MAT2016-76824-C3-1-R. M.J. and J.G.-H acknowledge financial support from the Spanish Ministry of Economy and Competitiveness through The "María de Maeztu" Programme for Units of Excellence in R&D (MDM-2014-0377). M.J also acknowledges financial support from Universidad Autónoma de Madrid and Comunidad Autónoma de Madrid through the project SI1/PJI/2019-00055. J.P.-N., C.M. and J.M.D.T. acknowledge financial support from the Spanish MINECO through the projects MAT2017-82970-C2-1-R, MAT2017-82970-C2-2-R and RED2018-102627-T, from the Aragon Regional Government (Construyendo Europa desde Aragón) through the project E13_20R with European Social Fund funding. This project has received funding from the European's Union Horizon 2020 research and innovation programme under Grant No. 823717-ESTEEM3. J.P.-N. grant is funded by the Ayuda para Contratos Predoctorales para la Formación de Doctores (BES-2015-072950) of the Spanish MINECO with the participation of the European Social Fund.

References

1 Y. Martin and H. K. Wickramasinghe, *Appl. Phys. Lett.*, 1987, **50**, 1455–1457.

2 J. J. Sáenz, N. García, P. Grütter, E. Meyer, H. Heinzelmann, R. Wiesendanger, L. Rosenthaler, H. R. Hidber and H. J. Güntherodt, *J. Appl. Phys.*, 1987, **62**, 4293–4295.

3 O. Kazakova, R. Puttock, C. Barton, H. Corte-León, M. Jaafar, V. Neu and A. Asenjo, *J. Appl. Phys.*, 2019, **125** , 060901.

4 A. Schwarz and R. Wiesendanger, *Nano Today*, 2008, **3**, 28–39.

5 V. Panchal, H. Corte-León, B. Gribkov, L. A. Rodriguez, E. Snoeck, A. Manzin, E. Simonetto, S. Vock, V. Neu and O. Kazakova, *Sci. Rep.*, 2017, **7,** 7224.

6 H. Corte-León, B. Gribkov, P. Krzysteczko, F. Marchi, J. F. Motte, H. W. Schumacher, V. Antonov and O. Kazakova, *J. Magn. Magn. Mater.*, 2016, **400**, 225–229.

7 R. Nagatsu, M. Ohtake, M. Futamoto, F. Kirino and N. Inaba, *AIP Adv.*, 2016, **6**, 056503.

8 M. Castagné, M. Benfedda, S. Lahimer, P. Falgayrettes and J. P. Fillard, *Ultramicroscopy*, 1999, **76**, 187–194.

9 H. Mattiat, N. Rossi, B. Gross, J. Pablo-Navarro, C. Magén, R. Badea, J. Berezovsky, J. M. De Teresa and M. Poggio, *Phys. Rev. Appl.*, in press.

10 H.-J. Chia, F. Guo, L. M. Belova, and R. D. McMichael, *Phys. Rev. Lett., 2012,* **108**, 87206.

11 I. Utke, P. Hoffmann, R. Berger, and L. Scandella, *Appl. Phys. Lett.*, 2002, **80**, 4792.

12 L. M. Belova, O. Hellwig, E. Dobisz and E. Dan Dahlberg, *Rev. Sci. Instrum.*, 2012, **83**, 93711.

13 M. Stiller, J. Barzola-Quiquia, P. D. Esquinazi, S. Sangiao, J. M. De Teresa, J. Meijer and B. Abel, *Meas. Sci. Technol,* 2017, **28**, 125401 .

14 M. Gavagnin, H. D. Wanzenboeck, S. Wachter, M. M. Shawrav, A. Persson, K. Gunnarsson, P. Svedlindh, M. Stöger-Pollach and E. Bertagnolli, *ACS Appl. Mater. Interfaces*, 2014, **6**, 20254–20260.

15 F. Wolny, T. Mühl, U. Weissker, A. Leonhardt, U. Wolff, D. Givord, *and* B. Büchner, *J. Appl. Phys.,* 2010, **108**, 1.

16 R. Puttock, H. Corte-Leon, V. Neu, D. Cox, A. Manzin, V. Antonov, P. Vavassori and O. Kazakova, *IEEE Trans. Magn.*, 2017, **28**, 2694324.

17 M. Jaafar, J. M. De Teresa, A. Asenjo , J. Pablo, E. Berganza, P. Ares, C. Magén, J. Gómez, "System for an atomic force microscope", patent PCT/ES2018/070709 and WO19086745.

18 J. Pablo-Navarro, C. Magén and J. M. De Teresa, *Nanotechnology*, 2016, **27**, 285302.

19 H. Plank, R. Winkler, C.H. Schwalb, J. Hütner, J.D. Fowlkes, P.D. Rack, I. Utke, M. Huth, *Micromachines* 2020, **11**, 48.

20 J. Pablo-Navarro, D. Sanz-Hernández, C. Magén, A. Fernández-Pacheco and J. M. De Teresa, *J. Phys. D. Appl. Phys.*, 2017, **50**, 18LT01.

21 J. Pablo-Navarro, C. Magén and J. M. De Teresa, *ACS Appl. Nano Mater.*, 2018, **1**, 38–46.

22 C. Lacovita, J. Hurst, G. Manfredi, P. A. Hervieux, B. Donnio, J. L. Gallani and M. V. Raste *Nanoscale*, 2020, **12**, 1842

23 M. Jaafar, L. Serrano-Ramón, O. Iglesias-Freire, A. Fernández-Pacheco, M. R. Ibarra, J. M. de Teresa and A. Asenjo, *Nanoscale Res. Lett.*, 2011, **6**, 1–6.

24 V. Neu, S. Vock, T. Sturm and L. Schultz, *Nanoscale*, 2018, **10**, 16881–16886.

25 H. J. Hug, B. Stiefel, P. J. A. van Schendel, A. Moser, R. Hofer, S. Martin, H.-J. Güntherodt, S. Porthun, L. Abelmann, J. C. Lodder, G. Bochi and R. C. O'Handley, *J. Appl. Phys.*, 1998, **83**, 5609–5620.

26 A. Asenjo, J. M. García, D. García, A. Hernando, M. Vázquez, P. A. Caro, D. Ravelosona, A. Cebollada and F. Briones, *J. Magn. Magn. Mater.*, 1999, **196**, 23–25.

27 R. Proksch, K. Babcock and J. Cleveland, *Appl. Phys. Lett.*, 1999, **74**, 419–421.

28 E. Berganza, M. Jaafar, M. Goiriena-Goikoetxea, J. Pablo-Navarro, A. Garcia-Arribas, K. Gusliyenko, C. Magen, J. M. de Teresa, O. Chubykalo-Fesenko, A. Asenjo, https://arxiv.org/abs/1803.08768.

29 R. E. Dunin-Borkowski, T. Kasama, A. Wei, S. L. Tripp, M. J. Hytch, E. Snoeck, R. J. Harrison and A. Putnis, *Microsc. Res. Tech.*, 2004, **64**, 390–402.

30 C. Phatak, L. de Knoop, F. Houdellier, C. Gatel, M. J. Hÿtch and A. Masseboeuf, *Ultramicroscopy*, 2016, **164**, 24–30.

31 C. Dietz, E. T. Herruzo, J. R. Lozano and R. Garcia, *Nanotechnology*, 2011 ,**22**, 125708.

32 P. Ares, M. Jaafar, A. Gil, J. Gómez-Herrero and A. Asenjo, *Small*, 2015, **11**, 4731–4736.

33 J. Sifford,K. J. Walsh,S. Tong,G. Bao and G. Agarwa, *Nanoscale Adv.*, 2019, **1**, 2348-2355

34 M.Jaafar, D. Martínez- Martín, M. Cuenca, J.Melcher, A. Raman, J. Gómez- Herrero, *Beilstein J. Nanotechnol.*, 2012, **3**, 336–344

35 Ó. Iglesias-Freire, M. Jaafar, E. Berganza and A. Asenjo, *Beilstein J. Nanotechnol.*, 2016, **7**, 1068–1074

36 A.B. Salunkhe, V.M. Khot, S.H.Pawar, *Curr. Top. Med. Chem*., 2014,**14** (5), 572-94

37 O. Guillaume-Gentil, E. Potthoff, D. Ossola, P. Dörig, T. Zambelli, and J.A. Vorholt, 2013, *Small*, **9,** 1904-1907

38 D. Wolf, L. A. Rodriguez, A. Béché, E. Javon, L. Serrano, C. Magen, C. Gatel, A. Lubk, H. Lichte, S. Bals, G. Van Tendeloo, A. Fernández-Pacheco, J. M. De Teresa and E. Snoeck, *Chem. Mater.*, 2015, **27**, 6771–6778.

39 I. Horcas, R. Fernandez, J.M. Gomez-Rodriguez, J. Colchero, J. Gomez-Herrero and A. M. Baro, *Rev. Sci. Instrum.*, 2007, **78**, 013705.